scientific reports

OPEN

Cyanidin-3-glucoside upregulated NDRG2 through the PI3K/AKT pathway to alleviate EMT and ECM in renal fibrosis

Qianxue Lu[1,2,5], Jin Liu[3,5], Yufeng Xiong[1,2,5], Jun Jian[1,2], Jingsong Wang[1,2], Zhiyuan Chen[1,2], Shanshan Wan[4✉], Xiuheng Liu[1,2✉] & Lei Wang[1,2✉]

Renal fibrosis is a critical progression of chronic kidney disease, and epithelial-to-mesenchymal transition (EMT) and extracellular matrix(ECM) deposition are crucial pathologic change of renal fibrosis, which still lacks of effective treatment. In this study, it was found that cyanidin-3-O-glucoside (C3G) could inhibit EMT and ECM activated by unilateral ureteral obstruction (UUO) and transforming growth factor-β1 (TGF-β1) stimulation. Moreover, N-Myc downstream-regulated gene 2(NDRG2), which involved in the progression of renal fibrosis, was down-regulated in vivo and in vitro model. However, C3G pretreatment could reverse the reductive expression of NDRG2. Furthermore, we found that the combined treatment of C3G and si-NDRG2 could reverse the decreased EMT and ECM, which induced by C3G treatment only. And the activation of Phosphatidylinositol 3-kinase (PI3K)/ Protein Kinase B (AKT) pathway significantly enhanced EMT and ECM, which was decreased by C3G treatment only in TGF-β1 induced Human Kidney 2 (HK-2) cells. In conclusion, our results demonstrated that C3G alleviated EMT and ECM by elevating NDRG2 expression through the PI3K/AKT pathway, indicating that C3G could be a potential treatment against renal fibrosis.

Keywords C3G, PI3K/AKT pathway, NDRG2, Renal fibrosis

Fibrosis is a common pathway of progressive chronic kidney disease (CKD) that finally leads to end-stage renal disease[1]. As one of the most severe diseases threatening human health worldwide, the incidence of CKD has been increasing in recent years, which is a heavy burden to patients and society[2]. Renal fibrosis plays a crucial role in the development of CKD. Exploring the complex relationship between CKD and renal fibrosis is of great significance for revealing the pathogenesis of the disease and developing effective therapeutic strategies. epithelial-to-mesenchymal transition (EMT) is the process by which epithelial cells lose their apical-basal polarity and gain migratory and invasive characteristics typical of mesenchymal cells[3,4]. Research has shown that the fibrotic process accompany with a gradual transformation of the cells to a mesenchymal phenotype, during which the epithelial cells begin to acquire specific markers unique, such as N-cadherin and α-smooth muscle actin (α-SMA). In addition, these cells produce and secrete mesenchymal matrix proteins during EMT, including fibronectin (FN) and collagen[5,6].

Transforming growth factor-beta (TGF-β) promotes the development of fibrosis, mediates EMT and activates mesenchymal cells to synthesize extracellular matrix (ECM), which provides an enabling microenvironment for the initiation and development of fibrosis[7]. In fibrotic diseases, TGF-β was upregulated and activated, which regulated fibroblasts' phenotype and function, inducing myofibroblast and promoting the deposition of extracellular matrix[8]. In this study, we established a unilateral ureteral obstruction (UUO) mouse model to investigate whether C3G could prevent renal fibrosis and how C3G exerts its inhibitory effect.

C3G, a member of the anthocyanin family (a subclass of flavonoids), is found in red berries, black rice, and red wine, which can reduce oxidative stress, enhance antioxidant systems, and suppress inflammation[9]. In previous studies, C3G has been shown to alleviate myocardial fibrosis by inhibiting the Toll-like receptor 4 (TLR4)/Nuclear factor kappa-B (NF-κB) pathway[10], reduce Reactive Oxygen Species (ROS) production

[1]Department of Urology, Renmin Hospital of Wuhan University, Wuhan 430060, Hubei, China. [2]Institute of Urologic Disease, Renmin Hospital of Wuhan University, Wuhan 430060, Hubei, China. [3]Department of Anesthesiology, Renmin Hospital of Wuhan University, Wuhan 430060, Hubei, China. [4]Department of Ophthalmology, Renmin Hospital of Wuhan University, Wuhan 430060, Hubei, China. [5]Qianxue Lu,Jin Liu,Yufeng Xiong contributed equally to this work. ✉email: ophwss@whu.edu.cn; drliuxh@whu.edu.cn; drwanglei@whu.edu.cn

1

and oxidative tissue damage to inhibit liver fibrosis[11], and decrease fibrosis in leiomyoma cells[12]. In diabetic nephropathy, studies have found that C3G inhibits renal fibrosis by alleviating mesangial inflammation and extracellular matrix (ECM) accumulation through fibrotic pathways[8].

Phosphoinositide 3-kinase (PI3K) is an enzyme involved in neural signal transduction. It catalyzes the phosphorylation of phosphatidylinositol (PI), as well as its derivatives, and can be activated by tyrosine kinase receptors, G protein-coupled receptors and ras protein-associated GDPase receptors[13]. As a downstream effector of PI3K, Protein Kinase B (AKT) is involved in various cellular processes, including cell proliferation, apoptosis, glucose metabolism, as well as cell migration and invasion[14]. Previous studies have demonstrated that the accumulation of ECM can be mitigated by inhibiting the activation of the PI3K/AKT signaling pathway[15]. Existing studies indicate that the PI3K/Akt signaling pathway contributes to renal fibrosis by regulating Mammalian target of rapamycin (mTOR) and Intercellular cell adhesion molecule-1 (ICAM1)[16–18]. For example, it has been reported that hyperforin can inhibit TGF-β1-induced EMT in renal epithelial cells by blocking the PI3K/AKT/ICAM1 signaling cascade, providing a potential basis for clinical treatment of renal fibrosis[16].

N-Myc downstream-regulated gene 2 (NDRG2) is a member of the NDRG family[19]. It is regulated by the PI3K/AKT signaling pathway and acts as one of its downstream molecules. NDRG2 regulates cell differentiation and proliferation in various tissues, including the brain, heart, liver, and kidneys[20,21]. Previous Research suggested that NDRG2 inhibited the activation of hepatic stellate cells (HSCs) by reducing the expression and phosphorylation of Smad3, thereby alleviating liver fibrosis[20]. Other study found that NDRG2 was significantly upregulated in normal proximal tubular cells compared to those in renal fibrosis[22], suggesting that it might inhibit this progression. However, the potential mechanism of NDRG2 in TGF-β1-induced human renal tubular epithelial cells still remains unknown.

Results

C3G ameliorated renal damage and fibrosis in UUO mice

In this experiment, the animal model of renal fibrosis was established by ligating the unilateral cis-ureter for 14 days to obstruct it. α-SMA is a renal fibrosis marker, and its expression reflects the degree of renal fibrosis. Compared with the sham-operated group, UUO resulted in obvious elevation of α-SMA and fibronectin expression, whereas those in the C3G group gradually decreased with the elevation of the C3G dose, and the optimal effect was reached at a dose of 200 mg/kg (Fig. 1A-B). Therefore, we chose 200 mg/kg for all subsequent experiments. In addition, HE staining showed that UUO caused renal parenchymal injury, primarily characterized by tubular dilatation and epithelial cell necrosis, while C3G treatment significantly attenuated the renal pathological damage (Fig. 1C-D). Masson staining showed that interstitial fibrosis was aggravated in UUO group, and interstitial fibrosis was improved in the C3G group (Fig. 1C-E). Immunohistochemistry showed α-SMA expression was increased in UUO group compared with sham-operated group, and C3G could reduce the elevated α-SMA expression induced by UUO (Fig. 1C-F).

### C3G ameliorated epithelial-mesenchymal transition and extracellular matrix deposition induced by UUO

EMT is a biological process in which epithelial cells undergo a specific program to transform into cells with a mesenchymal phenotype. Compared with the sham-operated group, the protein and mRNA levels of snail, vimentin and N-cadherin were significantly upregulated after UUO establishment, while C3G treatment reduced the increased expression induced by UUO, and protein and mRNA levels of the epithelial marker E-cadherin were significantly decreased, the C3G treatment indeed inhibited this process (Fig. 2A-C). An important marker of renal fibrosis is extracellular matrix deposition, which is reflected by the expression of FN, collagen I and collagen III. Compared with the sham-operated group, protein level and RNA level of FN, collagen I and collagen III were significantly increased after UUO establishment, whereas C3G treatment reduced their expression (Fig. 2D-F). These results suggested that C3G might exert a protective effect against renal fibrosis in vivo by reducing epithelial-mesenchymal transition and extracellular matrix deposition.

### C3G attenuated TGF-β1-induced fibrosis in human kidney 2 (HK-2) cells

Transforming growth factor β1, mainly regulating growth and differentiation, is usually used to induce fibrosis in vitro. The cytotoxicity of C3G was firstly detected using CCK-8 kit and the results indicated that this different concentration was almost non-cytotoxic (Fig. 3A). Then, our study found that as the concentration of C3G increased, it could reverse the decreased cell viability, which was caused by TGF-β1, and the best effect was at the concentration of 200μmol/L (Fig. 3B). Therefore, subsequent experiments were conducted at this concentration. Western blot showed that TGF-β1 could induce α-SMA expression, however, C3G pretreatment could reduce the increased α-SMA expression induced by TGF-β1 (Fig. 3C-D). The results of immunofluorescence staining were almost the same (Fig. 3E). Therefore, it suggested that C3G could attenuate fibrosis in HK-2 cells.

C3G ameliorated EMT and extracellular matrix deposition induced by TGF-β1 in HK-2 cells

To verify the effect of C3G on EMT/ECM in vitro, TGF-β1 was used subsequently in in vitro experiment. The protein and RNA level of snail, vimentin and N-cadherin were significantly upregulated after TGF-β1 treatment compared to the sham-operated group, while C3G treatment reversed this elevation. The epithelial marker E-cadherin, on the other hand, showed a significant decrease in protein and mRNA after TGF-β1 treatment, which was inhibited by C3G (Fig. 4A-C). Immunofluorescence showed the expression level of FN was significantly elevated after TGF-β1 treatment, and C3G effectively inhibited this process (Fig. 4D). The results of WB also showed that collagen I and III were increased in TGF-β1 group, however, C3G pretreatment could reduce the expression of collagen I and III induced by TGF-β1 (Fig. 4E-G). These results suggested that C3G also improved EMT/ECM in vitro.
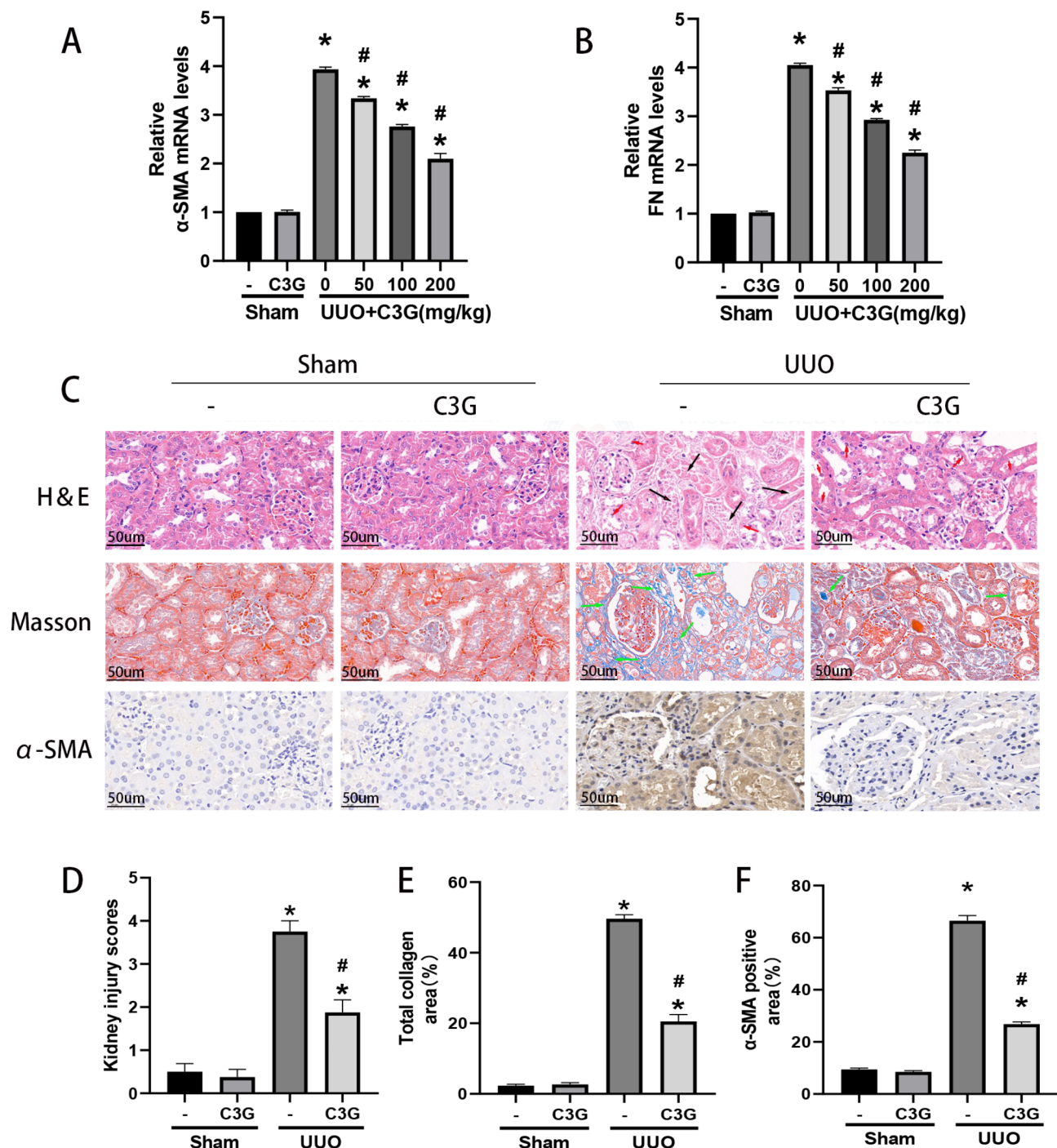
Fig. 1. C3G ameliorated renal fibrosis in UUO mice. (**A-B**) PCR detection of α-SMA and fibronectin in sham-operated and UUO groups after treatment with C3G. (**C**) Protective effect of C3G against renal tissue damage detected by H&E and Masson and α-SMA immunohistochemistry (×400). Black arrows represented tubular necrosis, red arrows represented detachment of tubular epithelial cells, and green arrows represented interstitial fibrosis. (**D**) The quantification of tubular damage score by H&E staining. (**E**) The quantification of total collagen area by MASSON staining. (**F**) The quantification of of α-SMA expression by immunohistochemistry. Values were expressed as the mean ± SEM. *$P < 0.05$, relative to the sham group. #$P < 0.05$, relative to the UUO group.
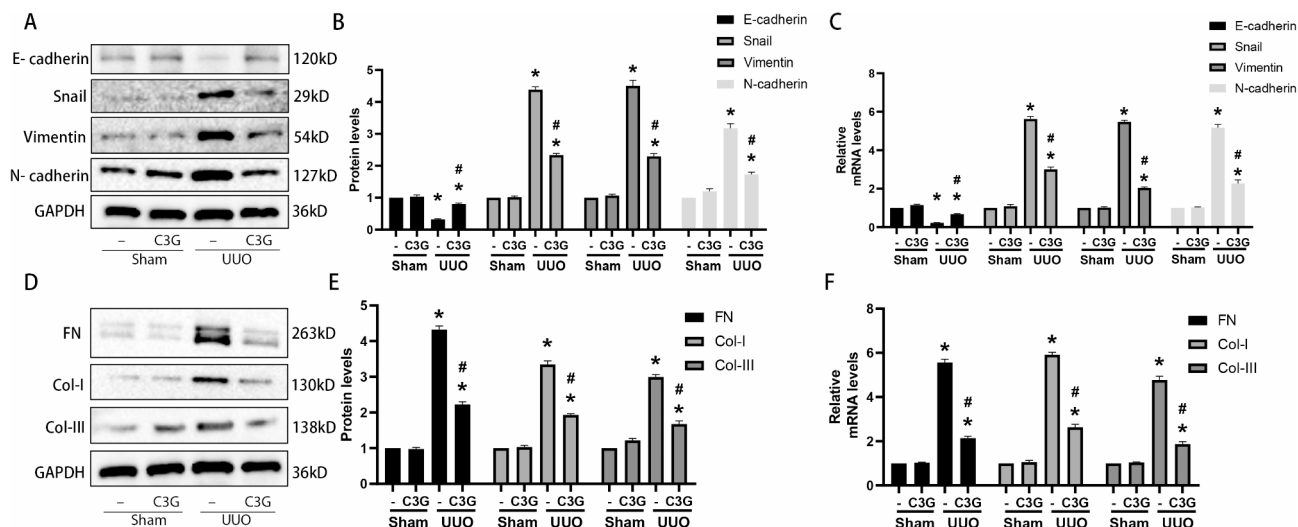
Fig. 2. C3G ameliorated UUO-induced epithelial-mesenchymal transition and extracellular matrix deposition. (**A**-**B**) E-cadherin, Snail, vimentin and N-cadherin protein level were examined in different groups, and the quantification of snail, vimentin and N-cadherin protein level relative to the sham-operated group. (**C**) mRNA levels of E-cadherin, snail, vimentin and N-cadherin were detected by real-time RT-PCR in different treatment groups. (**D**-**E**) FN, collagen I and collagen III protein level were examined in different groups, and the quantification of FN, collagen I and collagen III protein level relative to the sham-operated group. (**F**) mRNA levels of FN, collagen I and collagen III were detected by real-time RT-PCR in different treatment groups. Values were expressed as the mean ± SEM. *$P < 0.05$, relative to the sham group. #$P < 0.05$, relative to the UUO group.

NDRG2 was downregulated after UUO and TGF-β1 treatment

NDRG2 expression was detected at both mRNA and protein level and the results indicated that the expression of NDGR2 was significantly attenuated as UUO period prolonged (Fig. 5A-C). Immunohistochemical analysis was also performed and the reduction in positive areas of NDRG2 was easily observed in UUO group (Fig. 5D). And from the immunohistochemistry, it was found that NDRG2 was indeed expressed in proximal renal tubular epithelial cells, which was consistent with previous study[23]. Then cellular experiments were demonstrated that NDRG2 mRNA and protein were reduced as TGF-β1 treatment prolonged (Fig. 5E-H).

C3G reversed the NDRG2 reduction in in vivo and in vitro model

Compared with the control group, NDRG2 protein and mRNA were significantly decreased after TGF-β1 induction. However, C3G pretreatment significantly upregulated its expression in HK-2 cells (Fig. 6A-C). In addition, immunofluorescence showed that C3G pretreatment significantly enhanced the fluorescence intensity of NDRG2 protein in HK-2 cells after TGF-β1 induction (Fig. 6D). The in vivo experiments also showed similar results, as C3G could reverse the reduced NDRG2 expression in UUO mice (Fig. 6E-G).

C3G regulated EMT and extracellular matrix deposition induced by TGF-β1 through NDRG2

To further demonstrate whether C3G regulated EMT and extracellular matrix deposition through NDRG2, siRNA against NDRG2 was used. As shown, si-RNA significantly decreased NDRG2 protein and mRNA level (Fig. 7A-C). Compared with the TGF-β1 group, C3G pretreatment significantly reduced the expression of snail, vimentin and N-cadherin and increased the expression of E-cadherin, whereas combination with si-NDRG2 reversed the C3G-induced changes in expression (Fig. 7D). In addition, C3G significantly reduced the increased expression of FN, collagen I and collagen III caused by TGF-β1, which was reversed by the combination with si-NDRG2 (Fig. 7E). Therefore, C3G might exert the protective effect against EMT and extracellular matrix deposition induced by TGF-β1 through upregulation of NDRG2.

## C3G regulated NDRG2 expression, EMT and extracellular matrix deposition through the PI3K/AKT pathway in TGF-β1 induced HK-2 cells

To further explore the potential mechanism by which C3G regulated EMT and extracellular matrix deposition, we investigated the possible pathway involved. The PI3K/AKT pathway has been reported to play a key role in the regulation of NDRG2. As shown in Fig. 8A and B, TGF-β1 treatment activated the phosphorylation of PI3K and AKT, which was reversed by C3G treatment. We then used a specific AKT activator, SC79, to further validate the effect of C3G on PI3K/AKT pathway, and the results found that SC79 increased PI3K/AKT phosphorylation, whereas C3G attenuated this effect(Fig. 8C). The combination of C3G and PI3K/AKT activator SC79 could attenuate the elevated NDRG2 expression induced by C3G in TGF-β1 induced HK-2 cells (Fig. 8D). In addition, the activation of PI3K/AKT pathway significantly enhanced EMT and extracellular matrix deposition which was decreased by C3G in TGF-β1 induced HK-2 cells. (Fig. 8E and F). These results indicated that C3G regulated
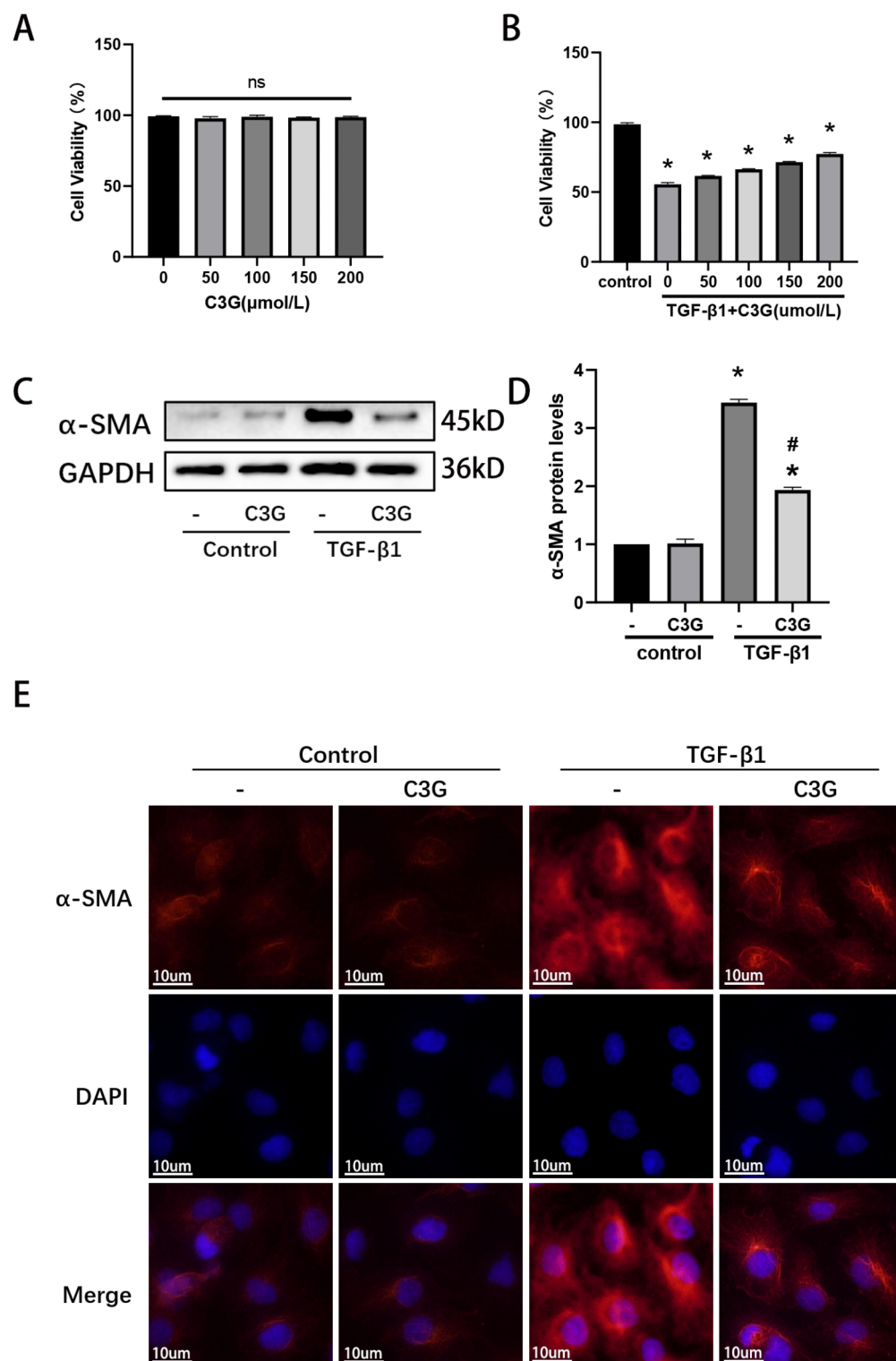
Fig. 3. C3G attenuated TGF-β1-induced fibrosis in HK-2 cells. (**A**) HK-2 cells were treated with different concentration (50, 100, 150, 200μmol/L) of C3G for 24 h, and then cell viability was detected by CCK-8; (**B**) HK-2 cells were treated with different concentrations (50, 100, 150, 200μmol/L) of C3G and TGF-β1 (5ng/mL), and cell viability was detected by CCK-8. (**C-D**) α-SMA protein level was examined by western blot in different treatment groups, and the quantification was showed as relative to the sham-operated group. (**E**) α-SMA Immunofluorescence was detected in each group. Values were expressed as the mean ± SEM. *$P < 0.05$, relative to the control group. #$P < 0.05$, relative to the TGF-β1 group.
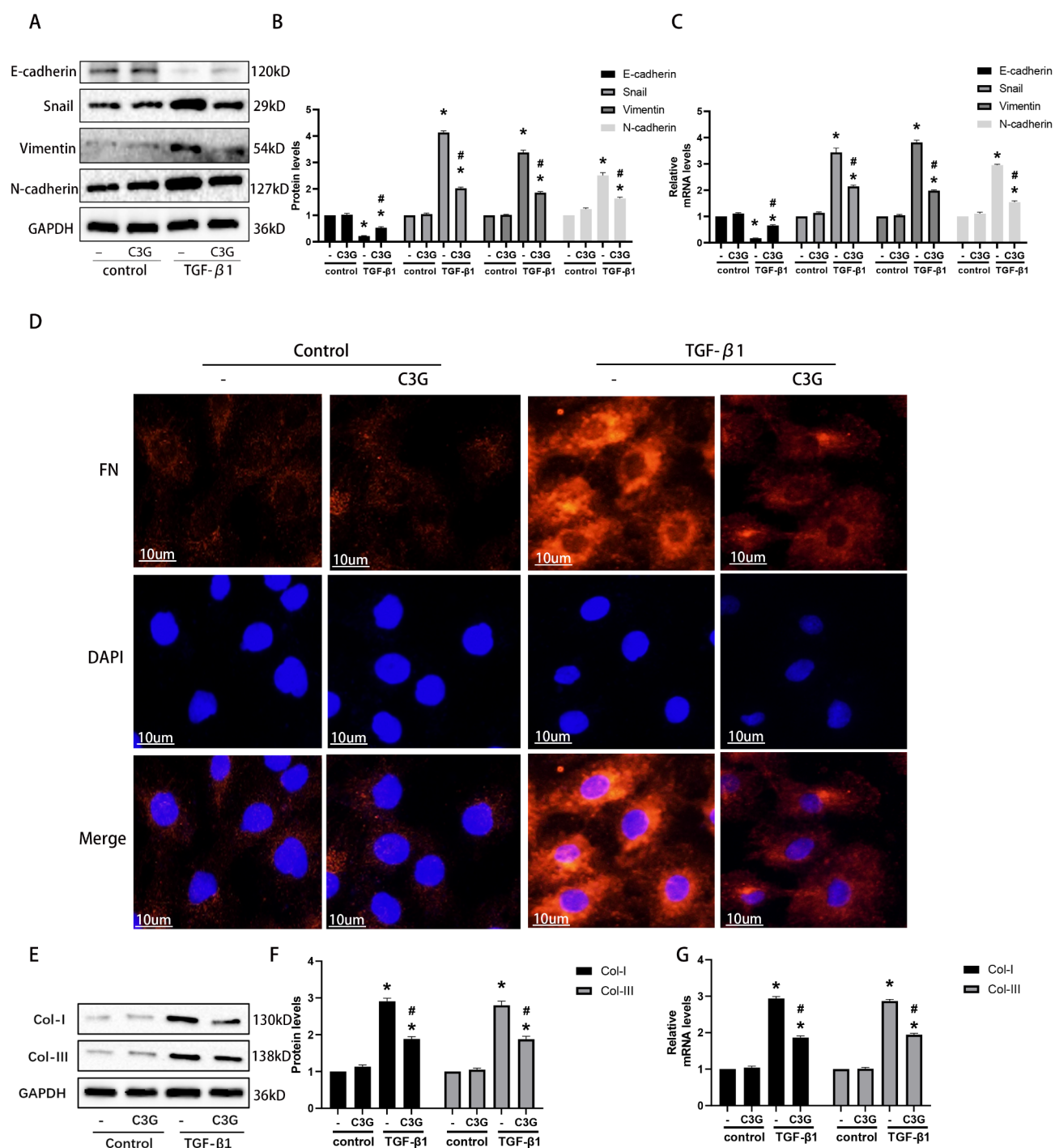
Fig. 4. C3G ameliorated EMT and extracellular matrix deposition induced by TGF-β1 in HK-2 cells. (**A-B**) E-cadherin, Snail, vimentin and N-cadherin protein level were examined by western blot in different groups, and the quantification of E-cadherin, snail, vimentin and N-cadherin was showed as relative to the sham-operated group. (**C**) mRNA levels of E-cadherin, snail, vimentin and N-cadherin were detected by real-time RT-PCR in different group. (**D**) FN immunofluorescence was detected and quantified. (**E-F**) Col-I and Col-III protein level were examined by western blot in different groups, and the quantification was showed as relative to the sham-operated group. (**G**) mRNA levels of Col-I and Col-III were detected by real-time RT-PCR in different group. Values were expressed as the mean ± SEM. $*P < 0.05$, relative to the control group. $\#P < 0.05$, relative to the TGF-β1 group.
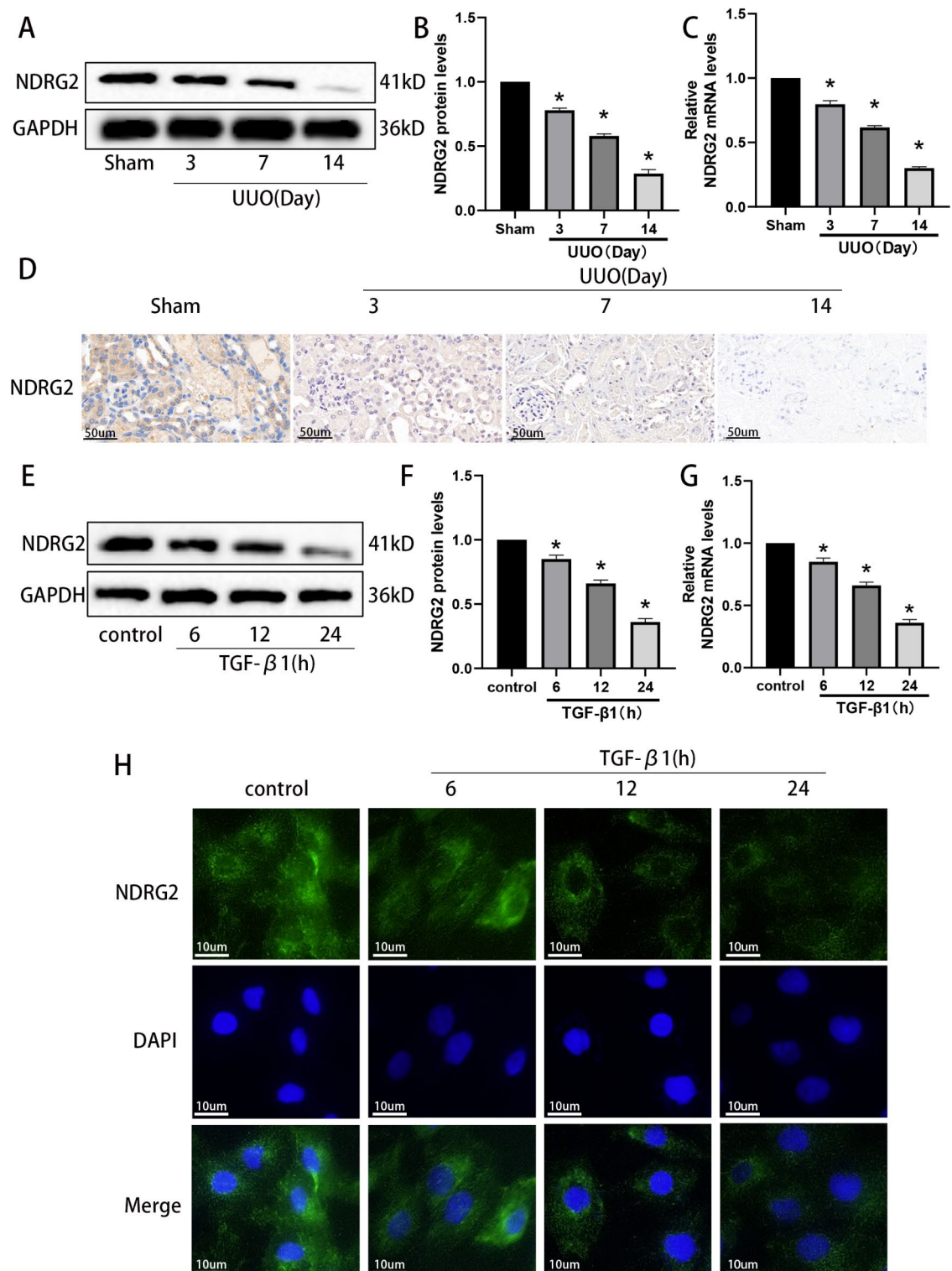
Fig. 5. NDRG2 was upregulated after UUO and TGF-β1 treatment. (**A**-**C**) NDRG2 protein and mRNA level were detected by western blot and RT-PCR at different period (3, 7 and 14 day) of UUO model establishment, and the quantification was showed as relative to the sham-operated group. (**D**) Immunohistochemical staining of NDRG2 was performed at different period (3, 7 and 14 day) of UUO model establishment. (**E**-**G**) NDRG2 protein and mRNA level were detected by western blot and RT-PCR at different period (6, 12, 24 h) of TGF-β1 treatment, and the quantification was showed as relative to the control group. (**H**) NDRG2 immunofluorescence was detected at different period (6, 12, 24 h) of TGF-β1 treatment. Values were expressed as the mean ± SEM. *$P < 0.05$, relative to the sham and control group.
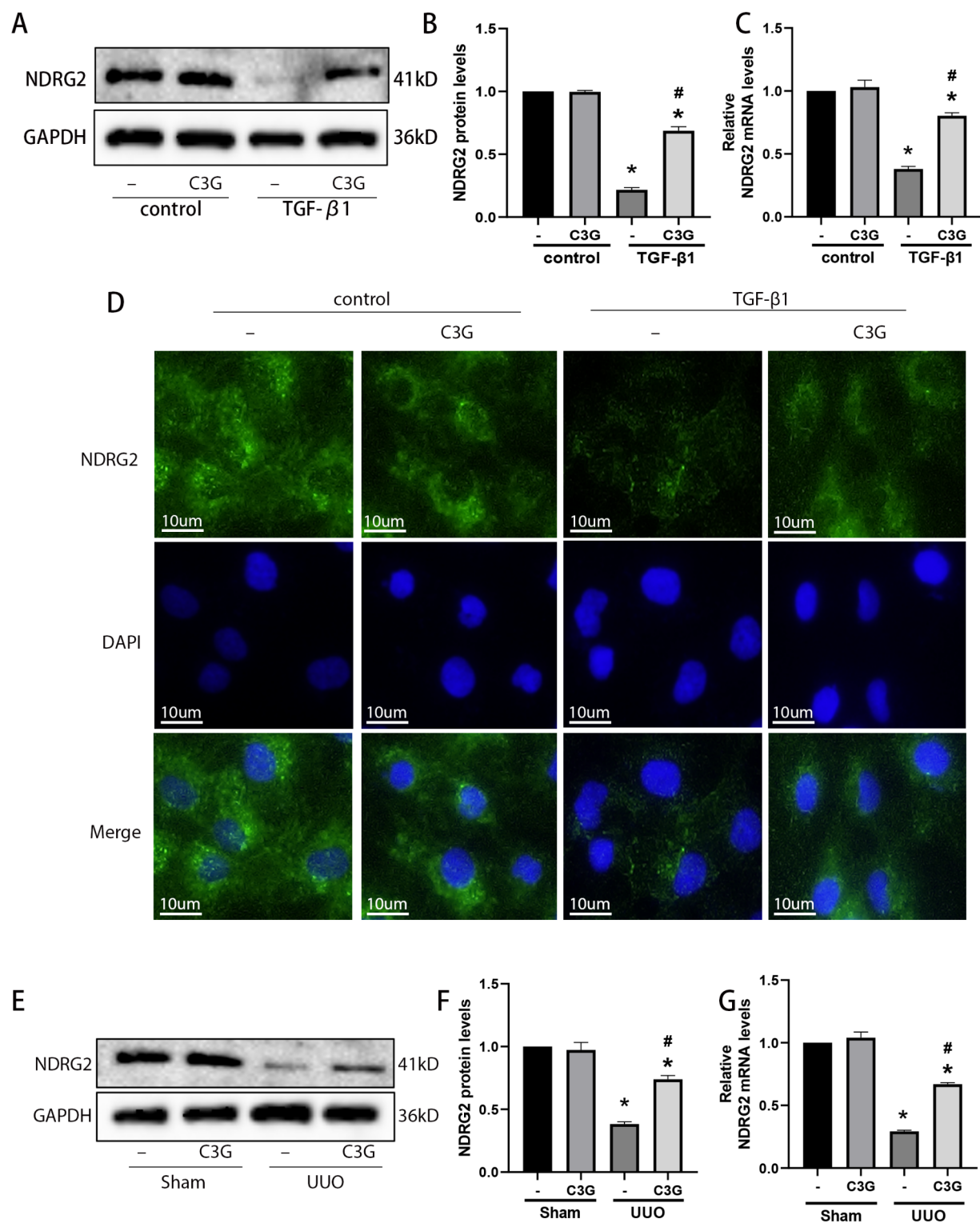
Fig. 6. C3G reversed NDRG2 reduction induced by UUO and TGF-β1 treatment. (**A**-**C**) NDRG2 protein and mRNA level were detected to investigate the effect of C3G on TGF-β1 induced HK-2 cells, and the quantification was showed as relative to control group. (**D**) Immunofluorescence was performed to see the localization of NDRG2. (**E**-**G**) NDRG2 protein and mRNA level were detected to demonstrate the effect of C3G on UUO mice, and the quantification was showed as relative to sham-operated group. Values were expressed as the mean ± SEM. *$P < 0.05$, relative to the sham and control group. #$P < 0.05$, relative to the UUO and TGF-β1 group.
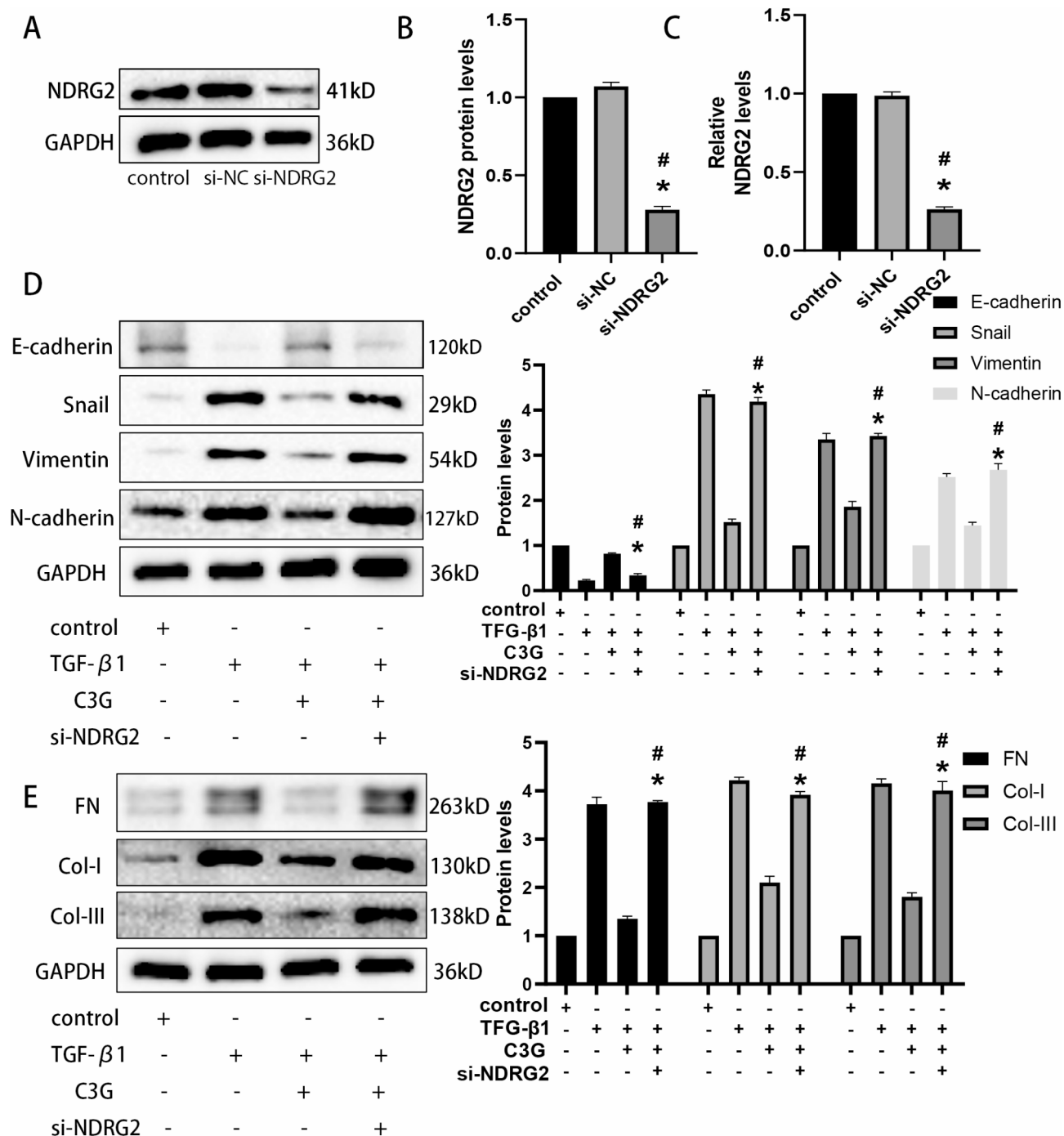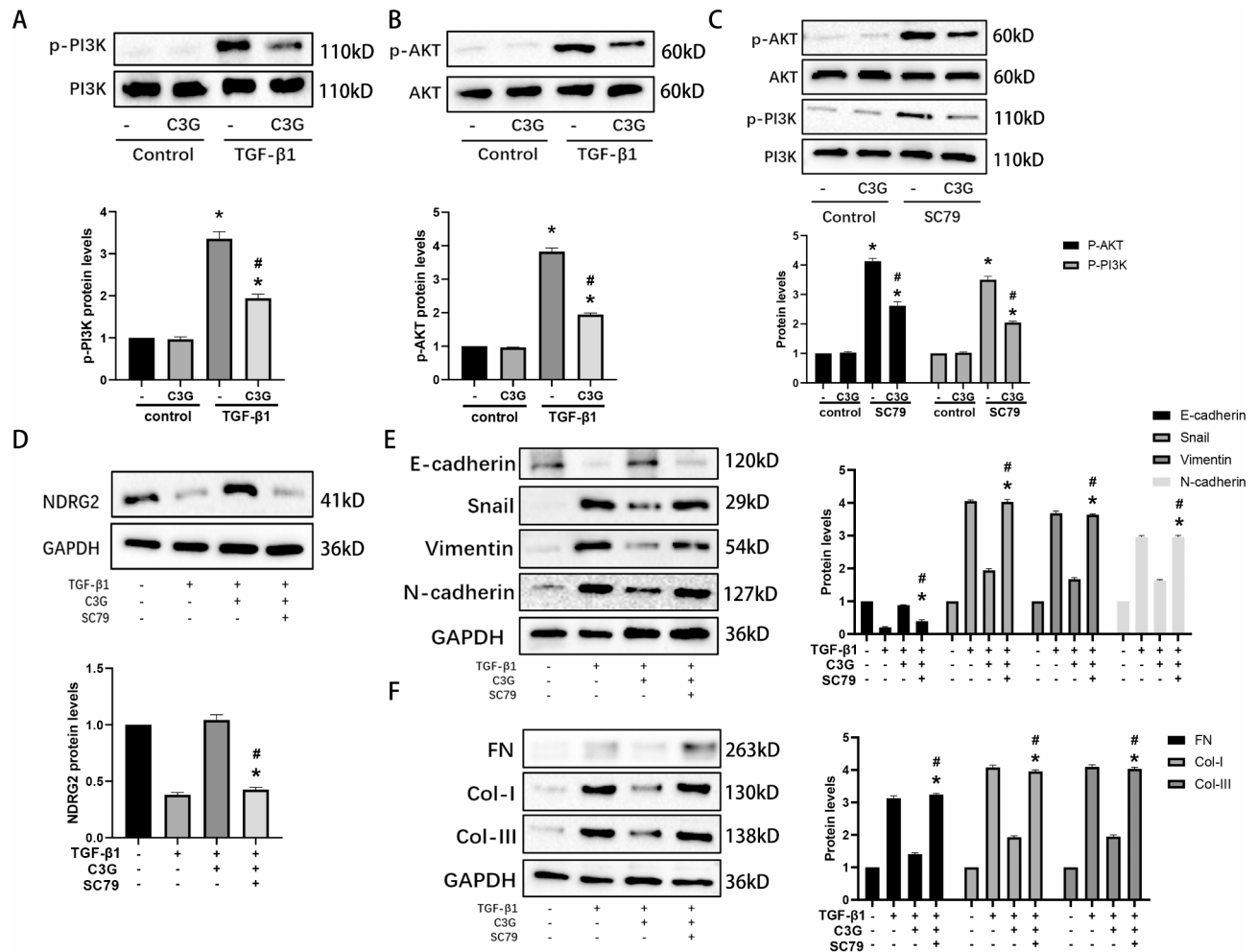
Fig. 7. C3G regulated EMT and extracellular matrix deposition induced by TGF-β1 on HK-2 cell through NDRG2. (**A**-**C**) NDRG2 protein level was detected by western blot and real-time PCR after si-NDRG2 transfection. (**D**) E-cadherin, Snail, vimentin and N-cadherin protein level were examined in different groups, and the quantification was shown as relative to the control group. (**E**) FN, Col-I and Col-III protein level were examined in different groups, and the quantification was shown as relative to the control group. Values were expressed as the mean ± SEM. *$P < 0.05$, relative to the control group. #$P < 0.05$, relative to the TGF-β1 + C3G group.

NDRG2 expression, EMT and extracellular matrix deposition through the PI3K/AKT pathway in TGF-β1 induced HK-2 cells.

Discussion

Fibrosis is characterized by the excessive accumulation of collagen and other ECM proteins in damaged tissues[24], leading to structural alterations and functional impairment[25]. EMT and ECM deposition play pivotal

Fig. 8. C3G regulated NDRG2 expression, EMT and extracellular matrix deposition through the PI3K/AKT pathway in HK-2 cells. (**A**-**B**) The expression of PI3K, p-PI3K, AKT, p-AKT and the quantification were shown after C3G treatment in TGF-β1 induced HK-2 cells. (**C**) Western blot and quantification of the effect of the combination of C3G and SC79 (PI3K activator, 20 μM) on PI3K/AKT expression. (**D**) The combination of C3G and SC79 (PI3K activator, 20 μM) could reverse the increased NDRG2 expression induced by C3G on TGF-β1 treated HK-2 cells. (**E**) The combination of C3G and SC79 (PI3K activator, 20 μM) could reverse the increased EMT induced by C3G on TGF-β1 treated HK-2 cells. (**F**) The combination of C3G and SC79 (PI3K activator, 20 μM) could reverse the increased extracellular matrix deposition induced by C3G on TGF-β1 treated HK-2 cells. Values were expressed as the mean ± SEM. *$P < 0.05$, relative to the control group. #$P < 0.05$, relative to the TGF-β1 + C3G group.

role in renal fibrosis[26]. EMT promotes the transformation of epithelial cells into mesenchymal cells, while ECM deposition exacerbates the structural and functional damage to renal tissues[27,28]. These processes are interrelated and collectively drive the progression of CKD and the exacerbation of renal fibrosis. And TGF-β1 is the vital cytokine to drive CKD-associated renal fibrosis[29,30]. In our study, it was found that EMT and ECM-related proteins were significantly upregulated in UUO mice and HK-2 cells, which was consistent with the previous.

Renal fibrosis, the main process involved in the progression of CKD to end-stage renal disease, is a serious clinical problem with high morbidity[31]. Many plant compounds, including celastrol and Poria cocos, have been found to effectively inhibit renal fibrosis[32,33]. Previous studies have indicated that C3G can attenuate fibrosis in various animal models, including those of diabetic nephropathy, CCl4-induced liver fibrosis, and non-alcoholic steatohepatitis-related fibrosis[9,34–36].In our study, we observed that different concentration of C3G could alleviate renal fibrosis in UUO mice, as demonstrated by reduction of α-SMA expression. Further, we investigated whether C3G exert its protective effect against renal fibrosis through regulation of EMT and ECM deposition. The results showed that the protein and RNA levels of snail, vimentin, N-cadherin, fibronectin, collagen I and collagen III were significantly upregulated after UUO or TGF-β1 stimulation, while C3G treatment reduced the expression of EMT and ECM deposition protein. These results demonstrated that C3G protected against renal fibrosis in UUO mice through the regulation of EMT and ECM deposition.

NDRG2 is a critical regulatory factor in organic fibrosis. The expression of NDRG2 is negatively correlated with the activation of HSCs, which are central to the progression of liver fibrosis[20]. For instance, previous studies

have reported that NDRG2 can reduce liver fibrosis and improve liver function by preventing the phosphorylation of ERK and Smad3[37]. Meanwhile, Jin et al. demonstrated that the knockout of NDRG2 affected the protein and mRNA expression levels of EMT markers and ECM components, thereby promoting renal fibrosis[22]. Consistent with their finding, our results show that NDRG2 expression was decreased in UUO mice and TGF-β1 induced HK-2 cells. However, pretreatment with C3G significantly could elevate NDRG2 expression, which indicated that NDRG2 had the effect of anti-fibrosis. Furthermore, our study investigated whether C3G affected EMT and ECM deposition in renal fibrosis through the regulation of NDRG2. The results showed that compared with the TGF-β1 group, C3G pretreatment significantly alleviated the expression of snail, vimentin, N-cadherin, fibronectin, collagen I and collagen III. While the combination of C3G and si-NDRG2 reversed this reduction induced by C3G. Therefore, it was concluded that C3G might exert the protective effect against EMT and extracellular matrix deposition induced by TGF-β1 through upregulation of NDRG2.

The PI3K/AKT pathway plays a crucial role in the progression of renal fibrosis[38], which is a pivotal pathway in kidney diseases[39]. Several studies have demonstrated that this pathway is activated in various CKD models and contributes to fibrosis by promoting inflammation, epithelial-mesenchymal transition, and extracellular matrix deposition. Others indicated that PI3K/AKT pathway not only regulated cell proliferation and survival, but also amplified the TGF-β1 response to fibrosis, through the RAS/RAF/MEK/ERK signaling cascade[40–42]. In our study, it revealed that PI3K/AKT pathway was activated in UUO mice and TGF-β1 induced HK-2 cells, which was consistent with previous study. Next, our study investigated whether C3G regulate EMT and ECM deposition through the PI3K/AKT pathway. And the results showed that activation of PI3K/AKT pathway with SC79 could enhance EMT and extracellular matrix deposition which was decreased by C3G in TGF-β1 induced HK-2 cells. Also, other study found that PI3K/AKT was the upstream pathway of NDRG2 and we wondered whether C3G elevated NDRG2 expression through PI3K/AKT pathway in our study. The results showed that the combination of C3G and PI3K/AKT activator SC79 could attenuate the elevated NDRG2 expression induced by C3G in TGF-β1 induced HK-2 cells.

In conclusion, we identified the protective effect of C3G against renal fibrosis in this study. Further, we indicated that C3G attenuated renal EMT and ECM deposition by elevating NDRG2 expression through PI3K/AKT pathway. Overall, these results revealed that C3G might be a potential treatment against renal fibrosis.

Methods

Experimental animals and renal fibrosis model

Adult male C57 mice (20–25 g) were provided by the Experimental Animal Center of the Medical College of Wuhan University (Wuhan, China). The project was approved by the Wuhan University Laboratory Animal Committee and was performed according to routine animal care guidelines. All procedures were in accordance with the Guidelines for the Care and Use of Laboratory Animals, and reported in accordance with ARRIVE guideline. To establish animal model of renal fibrosis, all mice were completely anesthetized by pentobarbital (50 mg/kg, i.p.) and placed on a thermostat to maintain their body temperature. A median abdominal incision was made into the abdominal cavity to expose the left kidney, and the proximal ureter was ligated with a silk thread. The mice in control group were subjected to only a median abdominal incision without ligation of the ureter. After the model was established, C3G was dissolved in dimethyl sulfoxide and then intraperitoneally injected once a day for three days. The mice were fed and sacrificed on day 3, 7, and 14. The blood and kidney specimen were collected for subsequent experiments. The whole blood samples were obtained using cardiac puncture.

Cell culture

HK-2 was obtained from the American Type Culture Collection (ATCC, USA). DMEM medium, containing 10% fetal bovine serum, 0.05 mg/mL bovine pituitary extract, 50 ng/mL human recombinant epidermal growth factor, 100 U/mL penicillin, and 100 μg/mL streptomycin, was used to culture HK-2 cells. The incubator temperature was kept at 37 °C and the culture condition was set at 5% CO_2 and 95% air. Cells were inoculated into 6-well plates, and TGF-β1 (2 ng/mL) was added to treat the cells for 6 h, 12 h and 24 h for subsequent experiments. All compounds were dissolved by DMSO and added to the culture medium to form different concentrations.

Histological staining and immunohistochemistry

After fixing and embedding the kidney tissue and cutting into 4 μm thick sections, the slides were stained with hematoxylin and eosin (H&E). The results of quantification of kidney damage were evaluated by two experienced renal pathologists who were unknowing the treatment and group according to the rating criteria of Jablonski et al.[43].

For Masson staining, the sections were dewaxed to water and then stained with Weigert's Iron Hematoxylin Stain for 8 min. After differentiation with acidic ethanol differentiation solution for 15 s, the sections were re-blued for 5 min and stained with Lichon red magenta staining solution for 5 min. After that, it was washed with phosphomolybdic acid solution, weak acid working solution for 1 min, and then stained with aniline blue staining solution for 2 min, and finally dehydrated and transparent.

Immunohistochemistry was performed using the Polink-1 one-step polymer detection system (ZSGB-BIO, Beijing, China). Briefly, the staining was incubated with primary antibody, followed by incubation with an HRP-labeled secondary antibody, and then detected with the EnVision/HRP kit (Dako, Denmark).

Serum assays

1 ml of venous blood was taken from mice and the serum was obtained by centrifugation at room temperature and processed according to the manufacturer's instructions (Nanjing Jiancheng Co., China). Blood urea nitrogen (BUN) and serum creatinine (Cr) levels were calculated spectrophotometrically.

Western blot analysis

HK-2 cells and kidney tissues were homogenized in RIPA lysis buffer (Beyotime, Jiangsu, China) containing protease inhibitors to lyse the cells to obtain total protein. After that, the protein was separated by 10% sodium dodecyl sulfate-polyacrylamide gel electrophoresis (SDS-PAGE) and then transferred to PVDF membranes in an ice-water bath. Then it was incubated with primary antibody at 4 °C overnight and incubated with 5% skim milk for 1 h at room temperature. The membranes were washed three times with TBST for 20 min each, incubated for 2 h at room temperature with secondary antibodies. Finally, the results were visualized using chemiluminescent HRP substrate (Millipore, Billerica, MA, USA). Data analysis was performed using Image J software (NIH, USA) to quantify protein levels. Primary antibody was used at the following dilutions:α-SMA(1:1000,Proteintech,14395-1-AP); Snail (1:1000, Abcam, ab216347); Vimentin (1:1000,Proteintech, 60330-1-Ig); N-cadherin(1:1000,Proteintech, 22018-1-AP); FN(1:1000,Proteintech, 15613-1-AP); Col-I(1:1000,Proteintech, 67288-1-Ig); Col-III(1:500,Proteintech, 22734-1-AP); NDRG2(1:1000, Abcam, ab174850);GAPDH(1:1000,Proteintech, 10494-1-AP); AKT(1:1000,Proteintech, 10176-2-AP); p-AKT(1:1000,Proteintech, 66444-1-Ig); PI3K(1:500,Proteintech, 20584-1-AP); p-PI3K(1:1000,Cell Signaling, 13857 S).

Quantitative real-time PCR

Total RNA was first extracted from HK-2 cells or kidney tissues using Trizol reagent and reverse transcribed to cDNA using the PrimeScript™ RT kit (TaKaRa Biotech, Dalian, China). Quantitative real-time PCR was performed using an ABIViiA7DX system (Foster City, CA, USA) by 30 s at 95 °C, followed by 40 cycles of 95 °C for 5 s, 60 °C for 30 s, and 72 °C cycle for 20 s. GAPDH expression was used for all experiments.

The Immunofluorescence

The cells were firstly fixed with paraformaldehyde, permeabilized with permeabilizing solution for 10 min and incubated with sealing solution for 30 min. After that the primary antibody was incubated at 4 °C overnight, and Phosphate Buffered Saline (PBS) was rinsed three times. Then the fluorescent secondary antibody was incubated at room temperature for 1 h. Finally, the slides were sealed and processed with a sealer containing diamidino-2-phenylindole (DAPI). The results were observed by a fluorescence microscope.

Cell viability

Cell viability was assessed using the CCK-8 assay (Beyotime Biotechnology, #C0037). HK-2 cells were firstly inoculated into 96-well plates according to the manufacturer instruction. After 24 h, the cells were pretreated with different concentration of C3G (0, 50, 100, 150, 200 μmol/L) for 24 h. Then TGF-β1 was used to establish the in vitro model. After 24 h, cells were incubated with 10ul of CCK-8 reagent for 2 h. Finally, the cells were analyzed by a microplate reader (Molecular Devices, USA).

Small interfering RNA (siRNA) transfection

Transfection of siRNA was performed by Lipo8000 Transfection Reagent (Beyotime). HK-2 cells were transfected with NDRG2-specific siRNA for 6 h. Meanwhile, the negative control was transfected with non-targeting siRNA (Santa Cruz Biotechnology, Santa Cruz, CA, USA) for 48 h. All transfected siRNAs were at the concentration of 100 μM. The effect of siRNA transfection was determined by western blot.

Statistical analysis

Statistical analysis was performed using GraphPad Prism version 5.0 (GraphPad Software, USA). All values were expressed as mean ± standard error of the mean. One-way analysis of variance was used to analyze the differences between groups. $p < 0.05$ indicated that the difference was statistically significant.

Data availability

The data supporting the findings of this study are available from the corresponding author (ophwss@whu.edu.cn, drliuxh@whu.edu.cn, and drwanglei@whu.edu.cn) upon reasonable request.

References

1. Romagnani, P. et al. Chronic kidney disease. *Nat. Rev. Dis. Primer.* **3**, 17088 (2017).
2. Ruiz-Ortega, M., Rayego-Mateos, S., Lamas, S., Ortiz, A. & Rodrigues-Diez, R. R. Targeting the progression of chronic kidney disease. *Nat. Rev. Nephrol.* **16**, 269–288 (2020).
3. Thiery, J. P., Acloque, H., Huang, R. Y. J. & Nieto, M. A. Epithelial-mesenchymal transitions in development and disease. *Cell* **139**, 871–890 (2009).
4. Savagner, P. Leaving the neighborhood: molecular mechanisms involved during epithelial-mesenchymal transition. *BioEssays News Rev. Mol. Cell. Dev. Biol.* **23**, 912–923 (2001).
5. Kalluri, R. & Weinberg, R. A. The basics of epithelial-mesenchymal transition. *J. Clin. Invest.* **119**, 1420–1428 (2009).
6. Stone, R. C. et al. Epithelial-Mesenchymal transition in tissue repair and fibrosis. *Cell. Tissue Res.* **365**, 495–506 (2016).

7. Tsuda, T., Horio, F. & Osawa, T. The role of anthocyanins as an antioxidant under oxidative stress in rats. *BioFactors Oxf. Engl.* **13**, 133–139 (2000).

8. Li, J. et al. Purple corn anthocyanins dampened high-glucose-induced mesangial fibrosis and inflammation: Possible renoprotective role in diabetic nephropathy. *J. Nutr. Biochem.* **23**, 320–331 (2012).

9. Zheng, H. X. et al. Cyanidin-3-glucoside from black rice ameliorates diabetic nephropathy via reducing blood glucose, suppressing oxidative stress and inflammation, and regulating transforming growth factor B1/Smad expression. *J. Agric. Food Chem.* **68**, 4399–4410 (2020).

10. Chen, Y. F. et al. Purple rice anthocyanin extract. Protects cardiac function in STZ-induced diabetes rat hearts by inhibiting cardiac hypertrophy and fibrosis. *J. Nutr. Biochem.* **31**, 98–105 (2016).

11. Hao, R. et al. Preventive effect and mechanism of anthocyanins from Aronia melanocarpa Elliot on hepatic fibrosis through TGF-β/Smad signaling pathway. *Cell. Biochem. Biophys.* **80**, 737–745 (2022).

12. Islam, M. S. et al. An anthocyanin rich strawberry extract induces apoptosis and ROS while decreases Glycolysis and fibrosis in human uterine leiomyoma cells. *Oncotarget* **8**, 23575–23587 (2017).

13. Zhao, K., Li, Y., Wang, Z., Han, N. & Wang, Y. Carnosine Protects Mouse Podocytes from High Glucose Induced Apoptosis through PI3K/AKT and Nrf2 Pathways. *BioMed Res. Int.* 4348973 (2019). (2019).

14. Covarrubias, A. J., Aksoylar, H. I. & Horng, T. Control of macrophage metabolism and activation by mTOR and Akt signaling. *Semin Immunol.* **27**, 286–296 (2015).

15. Xu, W., Yang, Z. & Lu, N. A new role for the PI3K/Akt signaling pathway in the epithelial-mesenchymal transition. *Cell. Adhes. Migr.* **9**, 317–324 (2015).

16. Yang, S. et al. Hyperforin regulates renal fibrosis via targeting the PI3K-AKT/ICAM1 axis. *Cell. Signal.* **108**, 110691 (2023).

17. Li, D. et al. Hydroxychloroquine alleviates renal interstitial fibrosis by inhibiting the PI3K/Akt signaling pathway. *Biochem. Biophys. Res. Commun.* **610**, 154–161 (2022).

18. Li, R. et al. Fufang Shenhua tablet inhibits renal fibrosis by inhibiting PI3K/AKT. *Phytomedicine* **116**, 154873 (2023).

19. Melotte, V. et al. The N-myc downstream regulated gene (NDRG) family: diverse functions, multiple applications. *FASEB J. Off Publ Fed. Am. Soc. Exp. Biol.* **24**, 4153–4166 (2010).

20. Yang, J. et al. NDRG2 ameliorates hepatic fibrosis by inhibiting the TGF-β1/Smad pathway and altering the MMP2/TIMP2 ratio in rats. *PLoS ONE.* **6**, e27710 (2011).

21. Lee, K. W., Lim, S. & Kim, K. D. The function of N-Myc Downstream-Regulated gene 2 (NDRG2) as a negative regulator in tumor cell metastasis. *Int. J. Mol. Sci.* **23**, 9365 (2022).

22. Jin, Z., Gu, C., Tian, F., Jia, Z. & Yang, J. NDRG2 knockdown promotes fibrosis in renal tubular epithelial cells through TGF-β1/Smad3 pathway. *Cell. Tissue Res.* **369**, 603–610 (2017).

23. Zhao, Y. et al. ROS promote hyper-methylation of NDRG2 promoters in a DNMTS-dependent manner: Contributes to the progression of renal fibrosis. *Redox Biol.* **62**, 102674 (2023).

24. Yuan, Q., Tan, R. J. & Liu, Y. Myofibroblast in kidney fibrosis: Origin, activation, and regulation. *Adv. Exp. Med. Biol.* **1165**, 253–283 (2019).

25. Lovisa, S. et al. Epithelial-to-mesenchymal transition induces cell cycle arrest and parenchymal damage in renal fibrosis. *Nat. Med.* **21**, 998–1009 (2015).

26. Kriz, W., Kaissling, B. & Le Hir, M. Epithelial-mesenchymal transition (EMT) in kidney fibrosis: fact or fantasy? *J. Clin. Invest.* **121**, 468–474 (2011).

27. Kuma, A., Tamura, M. & Otsuji, Y. [Mechanism of and therapy for kidney fibrosis]. *J. UOEH.* **38**, 25–34 (2016).

28. Liu, Y. Cellular and molecular mechanisms of renal fibrosis. *Nat. Rev. Nephrol.* **7**, 684–696 (2011).

29. Meng, X. M., Nikolic-Paterson, D. J. & Lan, H. Y. TGF-β: The master regulator of fibrosis. *Nat. Rev. Nephrol.* **12**, 325–338 (2016).

30. Lee, J. H. & Massagué, J. TGF-β in developmental and fibrogenic EMTs. *Semin Cancer Biol.* **86**, 136–145 (2022).

31. Rayego-Mateos, S. & Valdivielso, J. M. New therapeutic targets in chronic kidney disease progression and renal fibrosis. *Expert Opin. Ther. Targets.* **24**, 655–670 (2020).

32. Guo, Z. et al. Poria cocos: Traditional uses, triterpenoid components and their renoprotective Pharmacology. *Acta Pharmacol. Sin.* 1–16. https://doi.org/10.1038/s41401-024-01404-7 (2024).

33. Tang, M. et al. Celastrol alleviates renal fibrosis by upregulating cannabinoid receptor 2 expression. *Cell. Death Dis.* **9**, 1–12 (2018).

34. Zhou, Y. et al. Cyanidin-3-O-β-glucoside inactivates NLRP3 inflammasome and alleviates alcoholic steatohepatitis via SirT1/NF-κB signaling pathway. *Free Radic Biol. Med.* **160**, 334–341 (2020).

35. Qin, Y. et al. Cyanidin-3-O-glucoside ameliorates diabetic nephropathy through regulation of glutathione pool. *Biomed. Pharmacother Biomedecine Pharmacother.* **103**, 1223–1230 (2018).

36. Jiang, X. et al. Cyanidin-3-O-β-glucoside purified from black rice protects mice against hepatic fibrosis induced by carbon tetrachloride via inhibiting hepatic stellate cell activation. *J. Agric. Food Chem.* **63**, 6221–6230 (2015).

37. Huang, H. et al. The active constituent from gynostemma pentaphyllum prevents liver fibrosis through regulation of the TGF-β1/NDRG2/MAPK axis. *Front. Genet.* **11**, 594824 (2020).

38. Wang, Y. et al. LYC inhibits the AKT signaling pathway to activate autophagy and ameliorate TGFB-induced renal fibrosis. *Autophagy* **20**, 1114–1133 (2024).

39. Li, R. et al. Fufang Shenhua tablet inhibits renal fibrosis by inhibiting PI3K/AKT. *Phytomedicine Int. J. Phytother Phytopharm.* **116**, 154873 (2023).

40. Meng, X., Nikolic-Paterson, D. J. & Lan, H. Y. TGF-β: the master regulator of fibrosis. *Nat. Rev. Nephrol.* **12**, 325–338 (2016).

41. De Borst, M. H. et al. Glomerular and tubular induction of the transcription factor c-Jun in human renal disease. *J. Pathol.* **213**, 219–228 (2007).

42. Gruden, G. et al. Mechanical stretch-induced fibronectin and transforming growth factor-beta1 production in human mesangial cells is p38 mitogen-activated protein kinase-dependent. *Diabetes* **49**, 655–661 (2000).

43. Jablonski, P. et al. An experimental model for assessment of renal recovery from warm ischemia. *Transplantation* **35**, 198–204 (1983).

Acknowledgements

Author contributions

Qianxue Lu designed the study, supervised the experiments and wrote the manuscript. Jin Liu and Yufeng Xiong was responsible for manuscript writing, as well as cell culture and transfection. Jun Jian and Jingsong Wang conducted the UUO model and Masson staining. Shanshan Wan and Lei Wang critically appraised the manuscript and offered intellectual insights. Zhiyuan Chen and Xiuheng Liu performed the experimental work and analysis and refined the manuscript. All authors read and approved the final manuscript.

Declarations

Competing interest
The authors declare no competing interests.

Additional information
Supplementary Information The online version contains supplementary material available at https://doi.org/10.1038/s41598-025-94918-x.

Correspondence and requests for materials should be addressed to S.W., X.L. or L.W.

Reprints and permissions information is available at www.nature.com/reprints.

Publisher's note Springer Nature remains neutral with regard to jurisdictional claims in published maps and institutional affiliations.